ESRF Experiment Report

Proposal title:

Tuning the magnetic properties of 2D molecule-based magnets via rational control of the layer-layer distance

Proposal code: CH-6409

Beamtime: **BM01** (01/12/2022–04/12/2022), **ID12** (17/01/2023–23/01/2023)

Main proposer: Vincent NADURATA
Co-proposers : Nathan YUTRONKIE, Rodolphe CLÉRAC

---

1. Introduction

The current record for the highest critical temperature T_c for a molecule-based magnet is 515 K, held by the network $Li_{0.7}[Cr^{II}(pyz)_2]Cl_{0.7}\cdot 0.25(THF)$ (**1**$^{\mathbf{Li}}$; pyz = pyrazine, THF = tetrahydrofuran).[1] The material is composed of two-dimensional (2D) layers of Cr^{II} centres and pyrazine ligands in a grid-like arrangement separated by THF, Li^+ ions, and Cl^- ions between the layers, with its magnetic properties stemming from the strong ferrimagnetic exchange between square-planar Cr^{II} centres mediated by bridging pyrazine radicals. An important step in taking these materials outside the laboratory and into real devices is determining whether the bulk properties are maintained at the nano- or single layer scale. It is with this in mind that we sought to prepare similar layered Cr-pyz networks with much larger distances between the 2D layers, as the behaviour of these materials would thus approach what might be expected from an isolated monolayer.[2] A secondary goal was also to achieve a chemical exfoliation of the layers by prising them apart with larger and larger intercalants.[3] We thus synthesised analogues to **1**$^{\mathbf{Li}}$ with intercalated Na^+, K^+, Rb^+, and Cs^+ instead of Li^+. The study of these materials, denoted respectively by **2**$^{\mathbf{Na}}$, **3**$^{\mathbf{K}}$, **4**$^{\mathbf{Rb}}$, and **5**$^{\mathbf{Cs}}$, will allow us to determine how the magnetic properties are affected as the distance between the layers is gradually increased.

This report concerns a structural and electronic investigation of **1**$^{\mathbf{Li}}$–**5**$^{\mathbf{Cs}}$ based on high-resolution powder X-ray diffraction (HR-PXRD) measurements at **BM01** as well as X-ray absorption near-edge structure (XANES) and X-ray magnetic circular dichroism (XMCD) measurements at **ID12**.

2. Experimental details

We note briefly that due to technical issues during the first two days of the **ID12** beamtime, we were unable to utilise the better part of these first two days for measurements. These issues were mentioned in further detail in the feedback form our group submitted for this experiment.

3. Synthesis and structural investigation

Compounds $\mathbf{1}^{Li}$–$\mathbf{5}^{Cs}$ are synthesised by reducing the 2D network $CrCl_2(pyz)_2$ with 2.1 eq. of the appropriate M(Ac) reducing agent ($M^+ = Li^+$, Na^+, K^+, Rb^+, Cs^+; $Ac^{\bullet-}$ = 1,2-dihydroacenaphthylenide).[1,4] The reaction takes place in THF over 4 days. We note that PXRD measurements on $\mathbf{4}^{Rb}$ and $\mathbf{5}^{Cs}$ taken at our home laboratory instrument revealed incredibly poor crystallinity and broad, almost uninterpretable signals, and so these samples were not taken to **BM01**.

The room temperature HR-PXRD diffractograms at a detector distance of 200 mm taken at **BM01** of $\mathbf{1}^{Li}$, $\mathbf{2}^{Na}$, $\mathbf{3}^{K}$ are displayed in Fig. 1 (left), with the previously reported indexation of the diffraction pattern of $\mathbf{1}^{Li}$ indicated ($\mathbf{1}^{Li}$ is indexed in the *Pmmm* space group, with a = 6.9239(9), b = 6.9524(2), and c = 8.478(2) Å).[1] Diffractograms were also measured at detector distances of 0 and 500 mm, and it was decided that at 200 mm, the data gave the best balance of a sufficient 2θ range and good resolution.

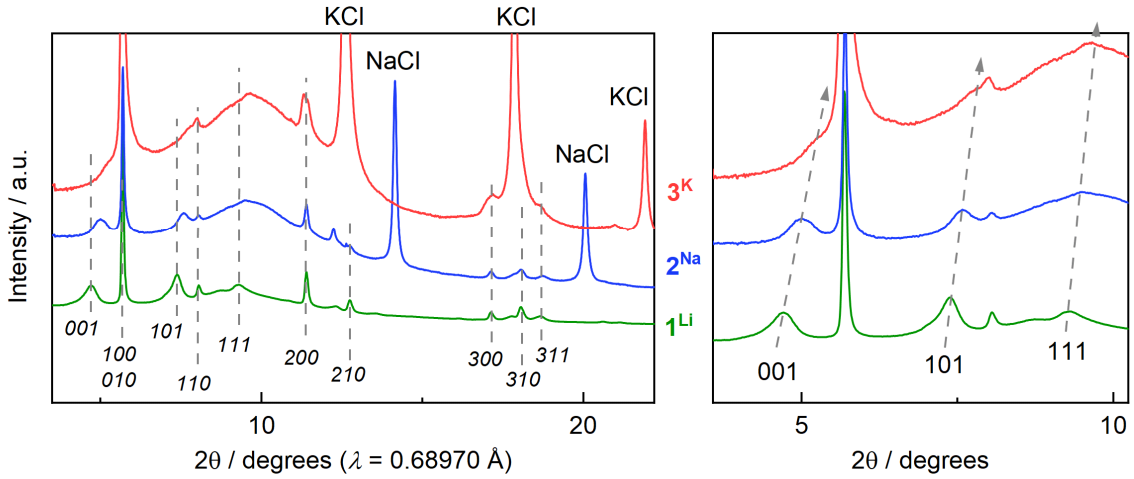

Figure 1. Left: HR-PXRD diffractograms of $\mathbf{1}^{Li}$, $\mathbf{2}^{Na}$, *and* $\mathbf{3}^{K}$ *collected at room temperature. Right: zoom of the same data depicting the shift of c-axis peaks to higher angles.*

Each of the *hk0* peaks in $\mathbf{1}^{Li}$ is reproduced in the diffractograms of $\mathbf{2}^{Na}$ and $\mathbf{3}^{K}$. As the Cr-pyz layers in $\mathbf{1}^{Li}$ are arranged in the *ab*-plane, these peaks directly report on the crystallographic order along these layers – hence, we may conclude that $\mathbf{2}^{Na}$ and $\mathbf{3}^{K}$ contain Cr-pyz layers similar to those in $\mathbf{1}^{Li}$. However,

the peaks relating to the *c*-axis, that is, those which report on the periodicity perpendicular to the planes, are shifted slightly between $\mathbf{1}^{\mathbf{Li}}$ and $\mathbf{2}^{\mathbf{Na}}$, and furthermore in $\mathbf{3}^{\mathbf{K}}$ become broadened and much weaker, indicating poor order in this direction for $\mathbf{3}^{\mathbf{K}}$. The general trend of these peaks from $\mathbf{1}^{\mathbf{Li}}$ to $\mathbf{2}^{\mathbf{Na}}$ to $\mathbf{3}^{\mathbf{K}}$ is towards higher angles, meaning that in fact as the alkali metal ion increases in size, the spacing between the Cr-pyz layers becomes smaller. Further evidence for this puzzling result is presented in the XANES spectroscopy section below.

The temperature-dependence of the diffractograms of $\mathbf{2}^{\mathbf{Na}}$ and $\mathbf{3}^{\mathbf{K}}$ was also investigated. Data were collected at 120 K to probe for any potential phase changes at low temperature: apart from slight shifts due to thermal contraction, the diffractograms were identical at 120 K and 300 K. For $\mathbf{2}^{\mathbf{Na}}$, due to the well-resolved nature of the *c*-axis reflections (see, for example, the *001* reflection in Fig. 1, right), a variable temperature study was also conducted to probe for the potential loss of THF from between the Cr-pyz layers, as well as for the decomposition of the material at higher temperatures. Similarly to $\mathbf{1}^{\mathbf{Li}}$, above 380 K the *c*-axis reflections of $\mathbf{2}^{\mathbf{Na}}$ begin to shift to higher energies as the temperature is increased.[1] Unlike for $\mathbf{1}^{\mathbf{Li}}$, however, this shift was also accompanied by a decomposition of the material, as evidenced by a decrease in the overall intensity of the diffractogram. Although this decomposition precludes a thorough analysis of the *c*-axis shift, we may conclude that as for $\mathbf{1}^{\mathbf{Li}}$, $\mathbf{2}^{\mathbf{Na}}$ contains THF molecules between the layers which begin to leave above 380 K.

As a final note, we also attempted to collect single-crystal X-ray diffraction data of $\mathbf{2}^{\mathbf{Na}}$ at BM01, but these efforts were ultimately fruitless as the samples either contained too many crystallites and simply gave diffraction rings, or no diffraction peaks were observed as the crystallite size was too small.

4. Electronic structure

To probe the oxidation state and geometry of the Cr centres in $\mathbf{2}^{\mathbf{Na}}$–$\mathbf{5}^{\mathbf{Cs}}$, Cr K-edge XANES spectra were measured at room temperature at **ID12**, using the spectrum of $\mathbf{1}^{\mathbf{Li}}$ as a reference.[1] These spectra are shown in Fig. 2.

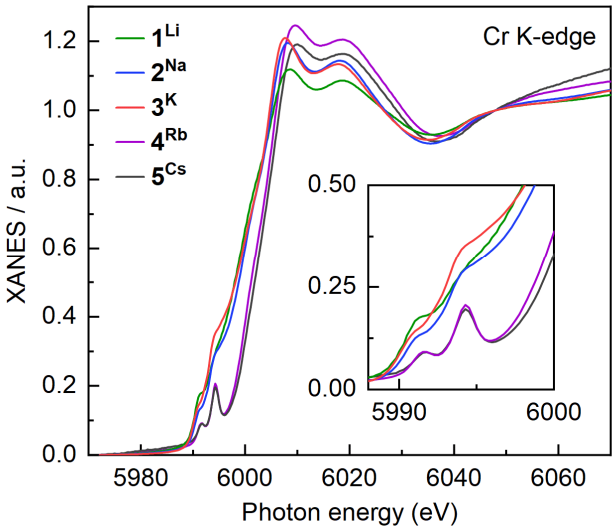

Figure 2. Normalised room temperature XANES spectra at the Cr K-edge of ***1***^{Li}*–****5***^{Cs}*. Inset: magnified view of the spectra in the near-edge region.*

The similarity between the profiles of the XANES spectra of **1**^{Li}, **2**^{Na}, and **3**^{K} in both the near-edge and rising edge regions indicates a similar oxidation state and coordination geometry. As we understand the previously characterised **1**^{Li} to exhibit square-planar Cr^{II} centres,[1] we can give the same assignment to **2**^{Na} and **3**^{K}. For **4**^{Rb} and **5**^{Cs}, although the pre-edge features at 5991 and 5994 eV are similarly located to those seen in **1**^{Li}–**3**^{K}, the overall intensity in this region is much weaker, and the position of the rising edge is shifted by around 3 eV higher in energy compared to **1**^{Li}–**3**^{K}. While this is consistent with a higher oxidation state for **4**^{Rb} and **5**^{Cs}, most likely Cr^{III}, we cannot discount the possibility of a decomposition of these highly air-sensitive materials, as a similar profile was observed for decomposed samples of **2**^{Na} and **3**^{K}.

The room temperature Cl K-edge spectra of **1**^{Li}–**5**^{Cs} are shown in Fig. 3. The features in the pre-edge region arise from mixing between the Cl *3p* orbitals and *3d* orbitals of other atoms. For **1**^{Li}–**3**^{K}, this is only possible between the Cl *3p* orbitals and the Cr *3d* orbitals, which in turn can only occur for Cl^- ions that are intercalated between the Cr-pyz layers. Hence, the intensity of the pre-edge signal gives an indication as to the ratio between intercalated Cl^- and extrinsic Cl^-. For the previously characterised **1**^{Li} it is known that Cl^- is solely present as intercalated ions, leading to a relatively strong pre-edge signal.[1] Moving to **2**^{Na}, this signal is much weaker, and for **3**^{K} it is barely present, if at all. This indicates that in **2**^{Na} some Cl^- is intercalated but most is present as extrinsic NaCl, while for **3**^{K}, practically all of the Cl^- is in the form of extrinsic KCl. We note that the NaCl and KCl are formed as byproducts of the reduction of $CrCl_2(pyz)_2$ by Na(Ac) and K(Ac) respectively. For **1**^{Li}, the analogous byproduct, LiCl, is soluble in the reaction solvent THF and is therefore washed away.[1]

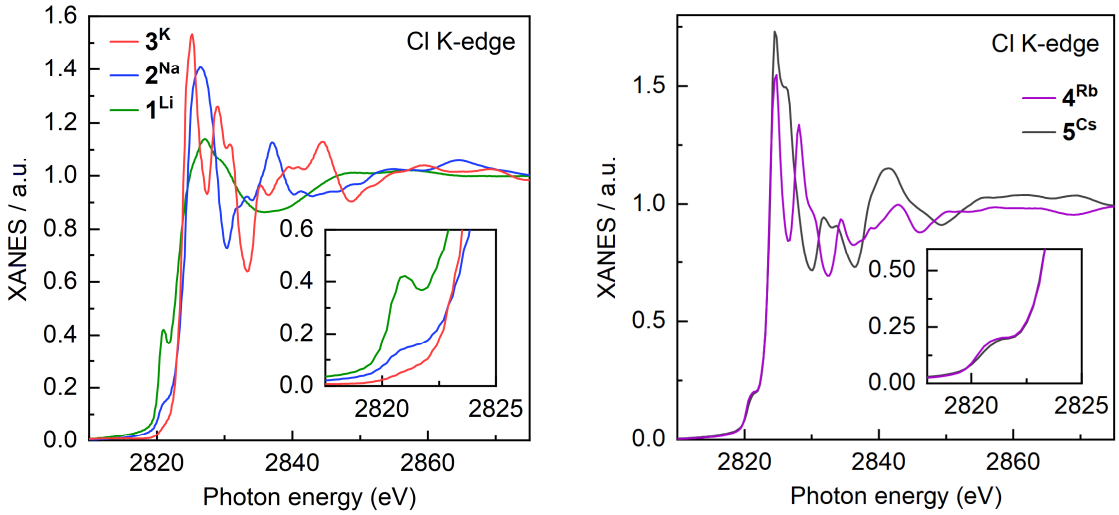

Figure 3. Normalised room temperature XANES spectra at the Cl K-edge of ***1***^{Li}*–*3^{K} *(left) and* ***4***^{Rb} *and* ***5***^{Cs} *(right). Inset: magnified view of the spectra in the near-edge region.*

For **4**^{Rb} and **5**^{Cs}, the same conclusions cannot be drawn as for their respective byproducts, RbCl and CsCl, mixing between the Cl *3p* and the alkali metal *3d* orbitals now becomes possible, as for Rb^+ and Cs^+ these orbitals are filled. In these materials, therefore, extrinsic Cl^- may also give pre-edge features in the Cl K-edge spectrum. Based on the trend that we observe from **1**^{Li}–**3**^{K}, with alkali metal intercalation already becoming difficult with K^+, we would expect Rb^+ and Cs^+ to be too large to enter between the Cr-pyz layers. Therefore, we associate the pre-edge feature in the spectra of **4**^{Rb} and **5**^{Cs} to mixing between the Cl *3p* and the alkali metal *3d* orbitals.

5. Magnetic properties

For **1**^{Li}, it has already been determined that its hysteretic behaviour stems from the anisotropy of the square planar Cr^{II} ions.[1] We sought to verify that this was also true for **2**^{Na}**–5**^{Cs} using XMCD measurements at variable field. The XMCD spectra of **2**^{Na} and **3**^{K} are shown in Fig. 4. Due to the probable decomposition of **4**^{Rb} and **5**^{Cs} that was evidenced by the Cr K-edge XANES spectra (Fig. 2), the XMCD of these two samples was not measured.

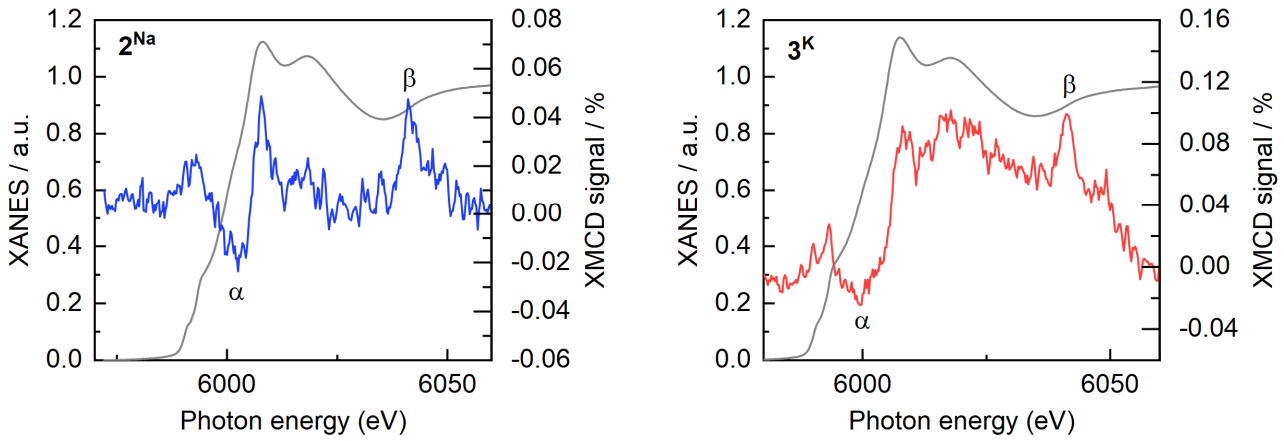

Figure 4. Normalised XANES spectra in grey of $\mathbf{2}^{Na}$ *(left) and* $\mathbf{3}^{K}$ *(right) with the corresponding XMCD spectra in colour shown as a percentage of the edge jump. The data are collected at 298 K, 5 T.*

The feature marked with α arises from polarisation of the Cr *4p* and *3d* orbitals by spin-orbit interactions, while the feature marked with β in the extended X-ray absorption fine structure (EXAFS) region is associated with multielectron excitations. These features agree well with the previously obtained XMCD spectrum of $\mathbf{1}^{Li}$, again confirming the similar local electronic structures of the Cr atoms between $\mathbf{1}^{Li}$, $\mathbf{2}^{Na}$, and $\mathbf{3}^{K}$.

As the intensity of the XMCD signal is proportional to the magnetisation of the Cr atoms, one can monitor the hysteretic behaviour of the system via the XMCD signal as a function of the field. For both $\mathbf{2}^{Na}$ and $\mathbf{3}^{K}$, the rising edge signal at 6000.7 eV was monitored as a function of the magnetic field from –17 to +17 T. The data for $\mathbf{2}^{Na}$ is displayed in Fig. 5, scaled to the previously obtained *M* vs. *H* curve of the bulk material. As the XMCD signal originates only from the magnetisation of the Cr centres (the spin-orbit polarisation of the radical pyrazine ligands should be sufficiently low such that they do not contribute to the XMCD signal), the similarity of its field dependence with the field dependence of the magnetisation indicates that the hysteretic properties of the material are dominated by the behaviour of the Cr^{II} centres.[1] The same behaviour was observed for the field dependence of the XMCD signal at 6000.7 eV of $\mathbf{3}^{K}$, confirming that the same interpretation is true for this material as well.

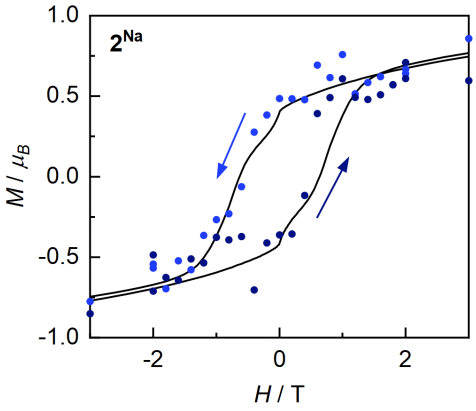

Figure 5. XMCD signal at 6000.7 eV, 298 K of $\mathbf{2^{Na}}$ *scaled to M vs. H curve of* $\mathbf{2^{Na}}$ *measured at 250 K.*

6. Summary and conclusions

The overarching goal of this project is to take the network $Li_{0.7}[Cr^{II}(pyz)_2]Cl_{0.7}\cdot 0.25(THF)$ and increase the distance between the Cr-pyz layers via chemical means, potentially towards exfoliation. A key step towards realising these goals is structural and electronic characterisation of the resulting materials. Through an in-depth HR-PXRD, XANES, and XMCD study at **BM01** and **ID12**, we have achieved a thorough picture of the structural and electronic characteristics of $\mathbf{2^{Na}}$–$\mathbf{5^{Cs}}$.

Despite the desired goal of increasing the interlayer distance, HR-PXRD indicated that as the alkali metal increased in size, this distance became lower. The Cl K-edge XANES measurements are consistent with the interpretation that as the alkali metal increases in size, less intercalation occurs, therefore resulting in a smaller interlayer distance. As for $\mathbf{1^{Li}}$, this interlayer distance could be modified by application of heat, with THF between the layers leaving above 380 K for $\mathbf{2^{Na}}$, as evidenced by a shift to higher angles of the *001* reflection with time and increasing temperature. Where for $\mathbf{1^{Li}}$ the material was stable up to 500 K, for $\mathbf{2^{Na}}$ a decomposition was observed much lower in temperature, with a decrease in intensity of the diffractogram observed from 380 K and above.

The Cr K-edge XANES measurements confirmed identical Cr oxidation states and coordination environments between $\mathbf{1^{Li}}$–$\mathbf{3^{K}}$, all possessing square-planar Cr^{II} centres. The dominant role of the Cr^{II} centres in the hysteretic behaviour of the compounds was demonstrated by XMCD measurements at varying field. Unfortunately, for $\mathbf{4^{Rb}}$ and $\mathbf{5^{Cs}}$, a probable decomposition of the materials precluded a proper analysis of their electronic structures.

Overall, the in-depth investigation outlined in the above has given us vital information as to the next steps needed in working towards the goals of this project. New synthetic strategies are required to drive the intercalation of larger alkali metal cations. We have also learnt that the magnetic properties of these materials are not significantly affected by changes in the layer-layer distance, an important knowledge in view of future efforts for rationally designing 2D networks for applications in next-generation devices.

References

1. Perlepe, P., Oyarzabal, I., Mailman, A., Yquel, M., Platunov, M., Dovgaliuk, I., Rouzières, M., Négrier, P., Mondieig, D., Suturina, E. A., Dourges, M.-A., Bonhommeau, S., Musgrave, R. A., Pedersen, K. S., Chernyshov, D., Wilhelm, F., Rogalev, A., Mathonière, C., & Clérac, R. (2020). Metal-organic magnets with large coercivity and ordering temperatures up to 242°C. *Science*, *370*(6516), 587–592.

2. Li, X., Lv, H., Liu, X., Jin, T., Wu, X., Li, X., & Yang, J. (2021). Two-dimensional bipolar magnetic semiconductors with high Curie-temperature and electrically controllable spin polarization realized in exfoliated Cr(pyrazine)$_2$ monolayers. *Sci. China Chem.*, *64*, 2212–2217.

3. Viculis, L. M., Mack, J. J., Mayer, O. M., Hahn, H. T., & Kaner, R. B. (2005). Intercalation and exfoliation routes to graphite nanoplatelets. *J. Mat. Chem.*, *15*(9), 974–978.

4. Pedersen, K. S., Perlepe, P., Aubrey, M. L., Woodruff, D. N., Reyes-Lillo, S. E., Reinholdt, A., Voigt, L., Li, Z., Borup, K., Rouzières, M., Samohvalov, D., Wilhelm, F., Rogalev, A., Neaton, J. B., Long, J. R., & Clérac, R. (2018). Formation of the layered conductive magnet $CrCl_2$(pyrazine)$_2$ through redox-active coordination chemistry. *Nat. Chem.*, *10*(10), 1056–1061.